The Eurasia Proceedings of Science, Technology, Engineering & Mathematics (EPSTEM)
ISSN: 2602-3199

The Eurasia Proceedings of Science, Technology, Engineering and Mathematics (EPSTEM), 2025

Volume 37, Pages 962-980

ICEAT 2025: International Conference on Engineering and Advanced Technology

Prosthetic Finger Design for Partial Hand Amputees: A Five-Bar Linkage Approach

Mennat Allah S. Yaseen
University of Technology - Iraq

Mohsin N. Hamzah
University of Technology - Iraq

Shaimaa H. Kamel
University of Technology - Iraq

Abstract: The passive prosthetic finger is designed, modeled, and functional tested with the five-bar closed-loop linkage mechanism for partial hand amputees. The prosthesis is designed with parametric CAD modeling, forward kinematic analysis, and hybrid manufacturing techniques. One single input with one actuation point gives controlled motion to a geometrically constrained mechanism without the need for motors or electronics. Materials used are biocompatible and resistant: 316L stainless steel and carbon fiber composite. Kinematic simulations proved a stable angular displacement (64.5° - 67.5°) and homogeneous velocity and acceleration profiles with loads of 0 to 100 N. The device was efficient, well-distributed with a little deformation. Functional tests like the Jebsen–Taylor and Box & Block tests proved the prosthesis's capability of performing dexterous tasks involving precision. The whole and under $200 budget cost for fabrication of the device made it worth using in low-resource places. These results support the five-bar linkage as a mechanically effective, anatomically accurate passive prosthetic solution. This is also inexpensive compared to costly myoelectric devices and promises of widespread clinical use.

Keywords: Prosthetic finger, Five-bar linkage, Passive mechanism, Biomechanical modeling, Partial hand amputation

Introduction

Those having a partial hand amputation face daunting challenges while trying to accomplish daily tasks, especially when those tasks require accurate and precise motor manipulation.This was addressed more by the works of Cuellar et al., (Ahmad et al., 2014) and Kristjansdottir et al., (Tchurukdichian et al., 2023) talk about both purposeful and psychosocial burden concerning the loss of hands—limitation of dexterity, altering body image, and being less self-reliant. The major causes of trauma and industrial accidents are in conflict zones or regions of low-resource availability, leading to loss of the fingers (Beckerle et al., 2019), (Kyberd 2022a). Therefore, under such conditions, there is a strong need for useful, reliable prosthetic devices as represented by Figure 1. The abovementioned devices work chiefly for the restoration of aesthetics and hence are referred to as prostheses. Neither do they have any mechanical functions of their own (Cutipa-Puma et al., 2023; Sheehan 2021; Kerver et al., 2023). Thus, acquiring these devices enables superficial enhancement and social reintegration. Aesthetically pleasing low-end prostheses, however, do not confer customized grasp or manipulation. In contrast, high-end myoelectric prostheses interpret EMG signals to perform movement control (Zheng et al., 2019; Sinskey & Spires 2024; Yaseen et al.,2025; Vaskov et al., 2022). These machines are capable of performing complex tasks but are very expensive, fragile, and due to a constant need for calibration, maintenance has become an expert-only job (Segil et al., 2021; Graham et al., 2023).

Figure 1. Anatomical structure of the human fingers showing bones, tendons, and joints.

Mechanical prostheses fall in between the cosmetic and electronic end of the spectrum in functionality. This describes a prosthesis that uses spring joints, tendon-operated mechanisms, and body-powered systems to imitate functional grips without battery or motor (Brand et al., 2019; Dunai et al., 2020; Efanov et al., 2022; Bregoli et al., 2022).Both research work done by Zheng et al. (2019), Nelson and Blauvelt (2022) suggest the possibility of hybrids of the aesthetic and functional demands. Also, Segil et al. (2021), Spaulding and Chen (2020) examined ratcheting prosthetic designs enabling passive locking and adjustable grip control, as illustrated in Figure 2.

A B C

Figure 2. Multi-articulated prosthetic hand demonstrating cylindrical grasp.
A. Michelangelo hand B. i-limb quantum XS; C. bebionic (small).

The individualization in prosthetic design has recently nourished much attention. The said authors utilized different designs: Kyberd (2022b), Beckerle et al. (2019), Ornaghi et al. (2023) use open-deliver 3-d printing and parametric modeling to create anatomy-adapted devices. These efforts display that low-fee, decentralized fabrication the usage of PLA, TPU, and stainless steel can meet numerous affected person goals throughout a range of environments (Braza & Martin 2020; Amaya-Rivas et al., 2024;Kamel et al., 2024). Software platforms along with SolidWorks and Fusion 360, allow specific CAD-based modeling even as ANSYS helps strain evaluation and deformation prediction (Cuellar et al., 2019;Semprini et al., 2022). The less widely explored vein of research on state-of-the-art closed-loop mechanical linkages on material programs for finger prostheses has seen perhaps the least of research. Planar five-bar mechanisms, notable for their predictable motion paths and compact footprints, are one possibility for prosthetic applications (Kristjansdottir et al., 2020; Sinke et al.,2022 ; Kumar et al., 2023). Such structures require only a single actuator, and Hamzah et al. (2013). The studies showed that the method becomes automatically stable due to geometric constraints (Hamzah et al., 2013; Shokur & Micera 2024).

So, prosthetic validation has kinematic modeling as one among its key areas. Kamel et al. (2023), Rand et al. (2024), Cuellar et al. (2019) and Kumar et al. (2023) evaluated mechanical movements of fingers by velocity and torque assessment. Dynamic simulations affirm that mechanical configurations can reflect biologically

feasible movement beneath passive or quasi-static conditions (Hall et al., 2020;Salman et al., 2020). The method by Shokur and Micera (2024), Bhaskaran and Zachariah (2022) in contact mechanics research proved mechanical integrity of the finger linkages under load transfer.

Traditionally, these control techniques went through muscle-driven structures to the combined approach interfaces. Hybrid structures combine mechanical linkages corresponding to primary sensors, thus generating feedback that is effective and reliable (Sinskey & Spires 2024; Kristjansdottir et al., 2020; Salman et al., 2020). Their specifications push for future research which would combine passive mechanics with embedded sensors and AI-based control. This would allow real-time changes in motion without heavy, inconvenient infrastructures (Amaya-Rivas et al., 2024; Munaretto & Loeffler, 2023; Bashir et al., 2022; Yaseen et al., 2025; Kamel et al., 2025).

Between prostheses for aesthetic purposes and ones with high technology, there is an apparent gap. An inexpensive, functional, anatomically accurate prosthetic finger model based on five-bar linkages is generated that provides potential view for indeed thrilling prospects. This study aims to fill the space between computer-aided design, finite element modeling, and material-based fabrication. It finishes the line of increasing prosthetic technologies with definite applied interest in both medical and humanitarian markets.

Methodology

System Design Flow Chart

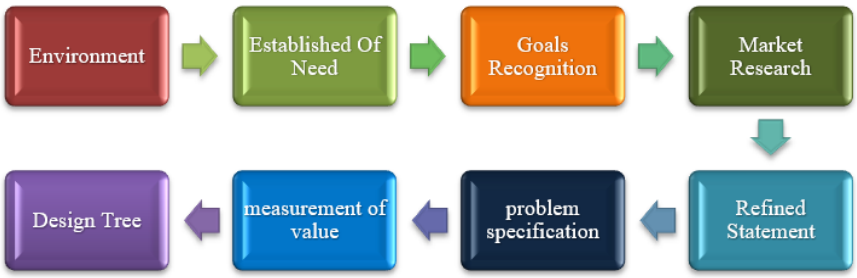

Below is an improved version of the design glide diagram with every step described:

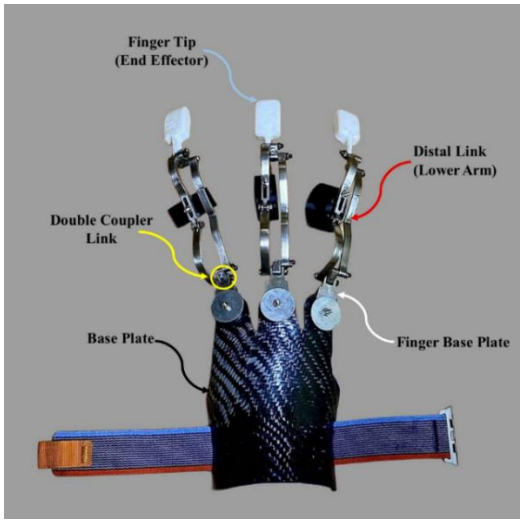

Features of the Finger Prosthesis	
Items	Specification
Size	240*120mm
Weight	147.7g
Material	Stainless steel 316 L
Power mechanical energy	Power mechanical energy
Price	200$

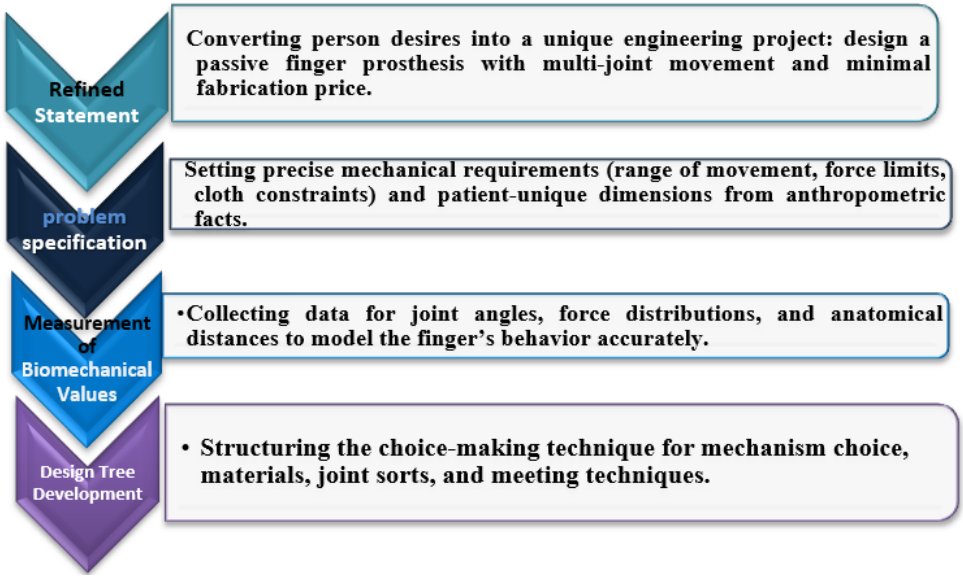

Figure 2. Design flow chart.

Design Tree of Prosthetic Finger for Mechanically Hand System

The schematics tree provided on the diagram shows the entire improvement of the prosthetic finger device, from initial virtual modeling to the final meeting of physical additives. Next step is 3D CAD modelling of palm, fingers and supporting ring systems. Thereafter the different manufacturing methods are followed through the virtual timeline. These include carbon fiber lamination for the socket, stainless steel 316L laser cutting and milling for mechanical linkages, and 3D printing using TPU and HYPER PLA filaments for adaptive fingertip components. The final phase integrates all elements - mechanical, bendy, and structural - into a completely functional prosthetic finger unit. This built breakdown allows for optimized planning, traceability, and manipulation of complexity in design across the interdisciplinary fabrication domain.

Design and Modeling

This bankruptcy provides advanced and realistic ways in designing and modeling a prosthetic finger mechanism especially indicated for partial hand amputees. The development is appropriately guided by the anatomical motion characteristics of the human hand and customized measurement data taken from the residual limb of the affected individual. While theoretical framework included mechanisms from the mechanical point of view, anatomical constraints were considered to give in-room functionality, adaptability, and individual comfort.

CAD design using SolidWorks 2022 allowed the geometric modeling of the finger mechanism and kinematic analysis to complete. The multi-jointed system mimics organic finger flexion and extension in the prosthesis, each joint is modeled as a revolute link. Major components such as base plate, proximal links, distal links, couplers, and tips all have been designed to allow for natural gripping motions and efficient load transfer.

The financial disaster also displays the application of forces and angular relationships across several articulation joints, specifically Joint 2, Joint 3, and Joint 4, which experience mechanical loading during usage. Thus, this modeling serves as the basis for dynamic simulations and structural analysis carried out later in the study. Equations governing joint action, torque balance, and angular displacement are derived from this model and validated through simulation and physical fabrication.

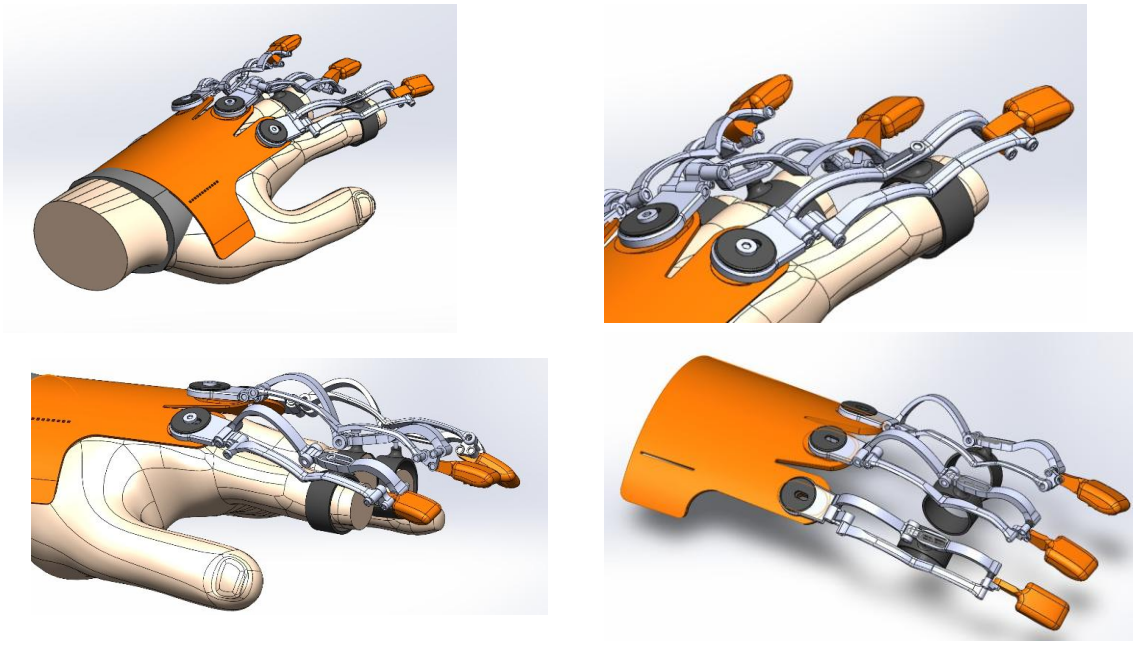

Figure 3. The images depict the completed SolidWorks model of the prosthetic hand assembly, showcasing finger mechanisms, joint placements, and the overall integration of components based on anatomical and mechanical design principles.

Conceptions of Finger Joints

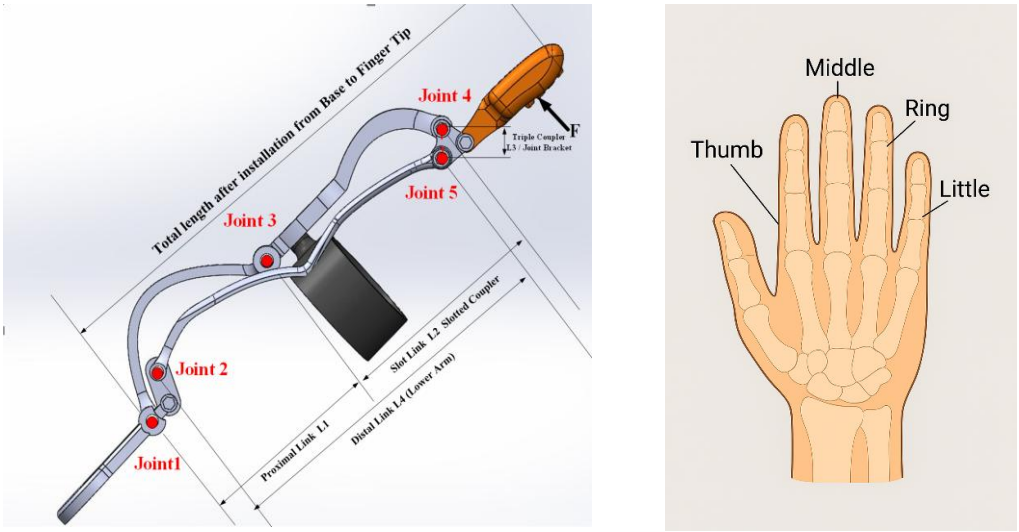

Figure 4. Length of finger design

It becomes all the more inevitable to clearly define the geometric parameters of prosthetic components to fully reclaim the human anatomical movement and access of a finger. Figure (3) shows the design of the prosthetic

finger, thus showing the 5 major joints and the 4 interlinked links of motion that replicate the natural movement of fingers. The segments Proximal Link (L1), Slot Link (L2), Triple Coupler (L3), and Distal Link (L4) undergo measurements and arrangements to enhance performance and manipulative skills. The desk below, Table (1) thereby presents actual dimensional values for three hands used within the final model in millimeters. The values ensure symmetry across the whole prosthetic layout, keeping in mind the power grip and natural actuation in daily chores. Each value corresponds to the particular mechanical part among the various joints, culminating in the total fixed finger length from base to fingertip as shown in Figure 4.

Physiological Actuation Cable-Free – Direct Muscle-to-Mechanism Interface

Movement is not governed by cables, electric motors, and other man-made transmitting systems but initiated directly by muscular force from the user, mostly from residual muscles remaining after partial amputation of a finger. Muscles such as the flexor digitorum profundus or superficialis are present, and if they are voluntarily activated, they will cause movement through the remaining structure of the finger. The way this is designed means that Link L4 or Joint 2 will mechanically connect to the palm or residual stump directly, so that any movement imparted is into the system by direct mechanical contact rather than flexible cables or the introduction of an intermediary component. Muscle contraction would push or rotate and start the closed-linkage construction as such, meaning initiating motion through slotted link (L2) controlled by the entire moving structure.

This is really a natural and intuitive outcome. The prosthetic fingertip is felt to be "attached" to the hand, almost effortlessly in a pretty good manner, and with great accuracy and comfort. The slotted constraint of L2 also makes that movement stable, secure, and limited to predictable pathways.

Closed Loop Planar Five-Bar Linkage with Slotted Coupler Mechanism Type

This particular mechanism can be thought of as one in the family of five-bar planar closed-loop rigid body linkages that utilize revolute joints and constrained motion paths; in this case, the closed loop is formed by four moving links and a fixed base connecting the end and initial points of the system as illustrated in Figure 4. This mechanism is different from open-chain mechanisms that do not constrain their endpoint with a loop that folds back on itself, between Joint 1 and Joint 2. The use of slotted coupler adds aside from the geometric constraints while the Triple Coupler with L3 terminates in a fixed point (Point P) receiving an external force. The design is for guided movement in well-defined bounds; thus, it finds applications in robotic fingers, assistive exoskeletons, and prosthetic digit joints. The design allows for high accuracy of output motion damaged by low-actuation input.

This configuration accommodates this five-bar mechanism.
-Input link L1 rotates from Joint 1 to Joint 3.
-Link L2 from Joint 3 to Joint 4 with a slot to restrict the motion of a sliding pin.
-Link L3 connects Joint 4 to Point P, a Triple Coupler bracket. It consists of:
-Joint 4 (rotation with L2)
-Joint 5 (rotation with L4)
-Point P (stable tip loaded by external force)
-Link L4 links from joint 5 to point P and is the distal segment power transmission to the end effector.
-A Ground Link is an intermediate link belonging to Joint 1 and Joint 2 and forming the closed loop frame.

Therefore, all motions are transmitted from one link to the next and not to create any spurious degrees of freedom, which ensures that everything is predictable.

Motion Characteristics and Degrees of Freedom

This mechanism supports one degree of freedom (DOF=1), that is, only one input-usually a rotation about Joint 1-is needed to drive the entire mechanism. The closed-loop topology of the arrangement ensures deterministic behavior of all other joints and links. The slotted joint of link L2 dictates the motion of the pin along a single linear trajectory relieved from transmission of any slack or motion ambiguity. In combining a single actuator with a high mechanical advantage and highly constrained geometry, the system converts the single rotation input into the carefully controlled and repeatable fingertip-level motion. It avoids instability or oscillation

unwanted and thus finds application in robotic fingers or exoskeleton linkages. Also, being planar and mechanically closed, it can withstand external forces at the endpoint without losing its orientation or position, which is critical in any wearable or load-carrying application.

Movement Behavior and Kinematic Function

The first event in motion commences with a turn in Joint 1, causing Link L1 to pivot around the joint. When Link L1 turns, it pushes/pulls Joint 3 and transmits the movement to Link L2. A slot in L2 allows the pin on L3 to move along a pre-chosen axis and not freely. Therefore, the pin is guided in its translational motion while Link L3 is rotating about Joint 4. Eventually, Link L3, as a Triple Coupler, transmits this restricted motion to Point P where the fingertip is located. Meanwhile, Link L4 links Joint 2 with Point P, stabilizing and supporting the mechanism by transferring force and torque across to the other side of the loop. In this way, the links work together to move the output tip along a complex but well-controlled path. In fact, all single-axis actuation, with all multidirectional fingertips, stability, and path control combined.

Force Transmission and Constraint Effects

Instead of applying external force at the joint, point P is a fixed point on Link L3. The torque introduced due to Point P rotation is about Joint 4, which gets transmitted in a reverse direction through Joints 3 and 1. The rigid coupling of Joint 2 to Joint 1 thus closes the loop and restricts displacement and grounds the system overall. It is essential to have the slot constraint along Link L2: it absorbs lateral reaction forces and allows movement only along the intended axis. Earlier dynamic error, energy loss, and misalignment are minimized.

Kinematic and Dynamic Analysis of the Mechanism (With Fixed Point P)

Symbol	Meaning	Unit
P	Fixed point on the rigid body of Link L3 (Triple Coupler) where **F** is applied	—
F	External force applied at point **P**	N
Fx, Fy	Components of **F** in X and Y directions	N
L_1, L_2, L_3, L_4	Lengths of links from each joint to the next	m
θ_1, θ_2, θ_3, θ_4	Angular position of each link	rad
ω_1, ω_2, ω_3, ω_4	Angular velocity of each link	rad/s
τ_1, τ_2, τ_3, τ_4	Torque at each joint	Nm
I_1–I_4	The moment of inertia of each link	kg·m²

The mechanism of blocking forces ensures that external loads (for example, gripping or pressing) are taken in mechanically and redistributed through the entire loop. This is extremely important in robotics or prosthetics, where load control must be reliable. This closed five-bar planar loop with slotted coupler and fixed application point for the force may, strikingly, be the most affordable, accurate, and durable mechanical solution to systems of constrained motion. Its innovative design can convert the stroke of a single input into stable guided motion with controlled response against external forces and with least degree of freedom, to best structural integrity.

Position of the End Effector (Point P)

From the point of view of the second stage of the analysis of a closed-loop five-bar system, this is an important spectrum of side motions that determines the position of the end effector (Point P) with respect to a base reference, which usually is Joint 1. This is done by employing a technique known as forward kinematics, which calculates the spatial position of all points on the mechanism from a given set of link lengths and joint angles. The calculations from the forward kinematic model then provide the mathematical basis for appropriately positioning the fingertip or system termination point.

The position vector $\vec{r}_P$ of the end effector is calculated as:

$$\vec{r}_P = \vec{r}_1 + L_1 \begin{bmatrix} \cos\theta 1 \\ \sin\theta 1 \end{bmatrix} + L_2 \begin{bmatrix} \cos\theta 2 \\ \sin\theta 2 \end{bmatrix} + L_3 \begin{bmatrix} \cos\theta 3 \\ \sin\theta 3 \end{bmatrix}$$

Symbol	Description	Unit
$\vec{r}_P$	Position vector of the end effector (Point P) in XY coordinates	[mm]
$\vec{r}_1$	Base reference position (Joint 1), often assumed as [0, 0]	[mm]
L1	Length of Link 1 (from Joint 1 to Joint 3)	[mm]
L2	Length of Link 2 (from Joint 3 to Joint 4)	[mm]
L3	Length of Link 3 (from Joint 4 to Point P)	[mm]
$\theta 1$	Angle of Link 1 with respect to the horizontal (X-axis)	[rad]
$\theta 2$	Angle of Link 2 relative to X-axis or previous frame (DH frame)	[rad]
$\theta 3$	Angle of Link 3 relative to X-axis or previous link	[rad]

The mechanism joints are represented with vectors of certain magnitudes Li, and oriented in the direction of the joint angle θi. The end effector absolute position (Point P) is determined by summing these consecutive vectors of Link 1, Link 2, and Link 3: each contributing to the overall displacement of the system from the base reference. In essence, each link provides a horizontal (X) component of Li·cos(θi) and a vertical (Y) component of Li·sin(θi). By the vector summation, the mechanism calculates the precise fingertip position according to the internal angular joint position, thus allowing fine and predictive fingertip position tracking.

Velocity of Point P

To observe the dynamic scheme of motion with respect to time of the end effector (Point P), one needs to analyze the velocity of the end effector due to the rotation of each link of the mechanism. Since the mechanism is a system of rigid bodies joined by revolute joints, the linear speed of Point P will result from combining all the angular velocities of the contributing links with their orientations in the differentiation of the position of Point P with respect to time. Through the kinematic analogy, the velocity expression for an end effector may be made in terms of the angular motion of the internal joint, thus allowing prediction and control of its dynamic performance. Time differentiation of this expression gives the velocity of Point P as a function of angular velocities of all links:

$$\vec{v}_P = J(\theta) \cdot \begin{bmatrix} w_1 \\ w_2 \\ w_3 \end{bmatrix}$$

$$\vec{V}_P = -\omega_1 . L_1 . \begin{bmatrix} \sin\theta 1 \\ -\cos\theta 1 \end{bmatrix} - \omega_2 . L_2 . \begin{bmatrix} \sin\theta 2 \\ -\cos\theta 2 \end{bmatrix} - \omega_3 . L_3 . \begin{bmatrix} \sin\theta 3 \\ -\cos\theta 3 \end{bmatrix}$$

Calculation of the Joint Angle of the Prosthetic Finger Mechanism

The characteristics of prosthetic finger joint angles are important to simulate true finger movements and to determine its proper functioning under numerous loads. This section outlines the geometric and vector calculations of the basic joint angles (θ_1 to θ_5) along the finger mechanism as shown in Figure 4. The finger comprises several curved links interconnected by revolute joints, from which, irrespective of the curvature, it is possible to derive angular relationships through vector projection and position coordinates.

The positions of all angles are calculated from the spatial coordinates of the respective joints by trigonometry and vector operations. These form a part of kinematic modeling and, hence, will also find application in simulation, control, and dynamic analyses of the prosthetic system. Let the position of each joint be defined as follows:

$\vec{P}_1, \vec{P}_2, \vec{P}_3, \vec{P}_4, \vec{P}_5$: Coordinates of Joint 1 through Joint 5.

$\vec{v}_i$: Vector between joints.

$\boldsymbol{\theta_1}$ Angle of the Proximal Link (L1), Angle between Joint 1 and Joint 3 concerning the global X-axis:

$$\theta_1 = \tan^{-1}\left(\frac{Y_1 - Y_0}{X_1 - X_0}\right)$$

$\boldsymbol{\theta_2}$ Angle between Proximal Link (L1) and Slotted Link (L2)

$$\vec{v}_1 = \vec{P}_3 - \vec{P}_1 \quad , \quad \vec{v}_2 = \vec{P}_4 - \vec{P}_3$$

$$\theta_2 = \cos^{-1}\left(\frac{\vec{v}_1 \cdot \vec{v}_2}{|\vec{v}_1|\,|\vec{v}_2|}\right)$$

$\boldsymbol{\theta_3}$ Angle between Slotted Link (L2) and Coupler (L3)

$$\vec{v}_3 = \vec{P}_5 - \vec{P}_4$$

$$\theta_3 = \cos^{-1}\left(\frac{\vec{v}_2 \cdot \vec{v}_3}{|\vec{v}_2|\,|\vec{v}_3|}\right)$$

$\boldsymbol{\theta_4}$ Orientation of the Slotted Link (L2) Relative to the base X-axis:

$$\theta_4 = \tan^{-1}\left(\frac{Y_3 - Y_1}{X_3 - X_1}\right)$$

$\boldsymbol{\theta_5}$ Angle between Proximal Link (L1) and Distal Link (L4)

$$\vec{v}_4 = \vec{P}_2 - \vec{P}_5$$

$$\theta_5 = \cos^{-1}\left(\frac{\vec{v}_1 \cdot \vec{v}_4}{|\vec{v}_1|\,|\vec{v}_4|}\right)$$

Torque Generated by the External Force $\vec{\boldsymbol{F}}$ *at Point P*

$$\vec{\boldsymbol{\tau}} = \boldsymbol{J}^{\boldsymbol{T}} \cdot \vec{\boldsymbol{F}}$$

At Joint 3 (pivot of Link L3):

$$\tau_3 = L_3.(F_x.\sin(\theta 3)) - F_y.\cos(\theta 3))$$

At Joint 2 (pivot of Link L2):

$$\tau_2 = \tau_3 + L_2.(F_x.\sin(\theta 2)) - F_y.\cos(\theta 2))$$

At Joint 1 (pivot of Link L1):

$$\tau_1 = \tau_2 + L_1.(F_x.\sin(\theta 1)) - F_y.\cos(\theta 1))$$

Alternatively, if using Link L4 directly (from Joint 4 to Point P):

$$\tau_4 = L_4.(F_x.\sin(\theta 4)) - F_y.\cos(\theta 4))$$

Such definitions for angles will be the basis for joint kinematic modeling and proof of prosthetic finger operation under standard constraint conditions. This would be particularly pertinent because of the non-linear link curvatures of the prosthetic model.

Total Dynamic Torque (Including Inertia)

$$\tau_i = I_i.\alpha_i + \vec{r}_i \times \vec{F}$$

Where:

τ_i total torque at joint *i*

I_i: moment of inertia of Link *i*

α_i: angular acceleration of Link *i*

$\vec{r}_i$: position vector from joint *i* to the point of application of the force

$\vec{F}$: external force applied at point P

Kinematic Constraint due to the Slot

Assumptions: Taking Link L2 to encompass a slotted guide, which is inclined at an angle ∅1, such that it receives a pin from Link L3. The point P represents the contact location between the pin and the slot surface.
A. Geometric Constraint Equation:
Point P must always lie along the direction of the slot. Mathematically:

$$(\vec{r}_P - \vec{r}_{slot}) \cdot \vec{n}_\perp = 0$$

Where:

- $\vec{r}_P$: position vector of the pin (from Link L3)
- $\vec{r}_{slot}$: position vector of the origin of the slot (in Link L2)
- $\vec{n}_{\perp=}\begin{bmatrix}-\sin\emptyset \\ \cos\emptyset\end{bmatrix}$ unit vector perpendicular to the slot direction

This constraint ensures that the pin can move only along the slot direction, and not outside of it.
B. Velocity Constraint:
Taking the time derivative of the geometric constraint:

$$\frac{\partial}{\partial t}[(\vec{r}_P - \vec{r}_{slot}) \cdot \vec{n}_\perp] = 0 \Rightarrow (\vec{v}_P - \vec{v}_{slot}) \cdot \vec{n}_\perp = 0$$

This implies that the component of the velocity perpendicular to the slot direction is zero, and that motion is allowed only along the slot axis.

Dynamic Analysis Involving the Slot

When analyzing forces and torques:

1- The permissible force at point P, denoted $\vec{F}_P$, has:

- Only one active component along the slot direction: $F_{\|}$
- The perpendicular component of the force becomes a reaction force, contributing nothing to motion

2. Torque Generated by Slot Force:

- If the distance between the rotational joint and the point P is r, then the torque resulting from the slot constraint is:

$$\tau_{slot} = r \times F_{\|}$$

In the dynamic equation of motion:

$$\tau_2 = I_2 \cdot \alpha_2 + \underbrace{r \cdot F_{\|}}_{Torque\ from\ slot\ force}$$

Where:

- τ_2: net torque at joint 2
- I_2: moment of inertia of Link 2
- α_2: angular acceleration of Link 2
- $F_{\|}$: active component of the force transmitted through the slot

Some theoretical considerations and analyses were required to include the entire mechanical structure of the prosthetic finger. The mechanism was anatomically scaled and biomechanically optimized for joint placement, link dimension, and force transmission in the mechanism. Kinematic and static analysis was further carried out to mathematically define angles, torque distribution, and motion behavior with the outcome of enabling motion of the prosthetic finger as near to a natural finger as possible.

With the theoretical considerations in place, the next chapter will now deal with implementing this into practice, on the other hand, provides the experimental methods, prototype fabrication, simulation outcomes, and physical experiments performed for verifying the performance and reliability of the proposed prosthetic system.

Results and Discussion

Functional Assessment of the Prosthetic Hand

Completely practical, the simulated prosthetic hand submission was at rigorous tests with a wide array of real-world manipulation item usage tasks. The consumer achieved managed grasping and dealing with of devices with varied geometries, masses, and cloth stiffness, such as plastic water bottles, digital items, lightweight packages, cylindrical cans, and interlocking toy blocks, as seen in Figure 5.

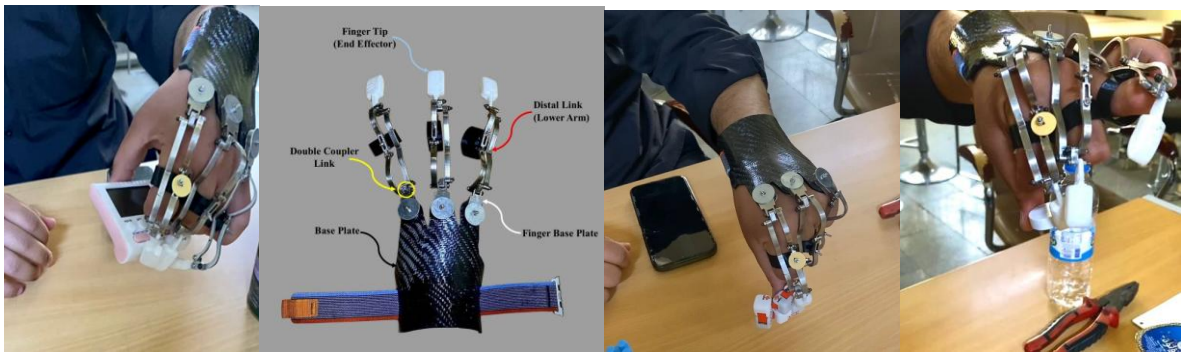

Figure 5. Application of standardized hand function tests (Jebsen–Taylor & Box and Block) on the fabricated prosthesis

The purpose of the experiments was to evaluate the working capabilities of the five-joint mechanical form and stainless-steel coupling machine under standard conditions of use. The fingers showed simple passive compliance to the objects, adjusting smoothly to the shape of each object. The coordinated motion of the coupler-based joints enabled stable programming of various types of grips, including three-finger close grip, pinch grip, and enveloping keep. During those tasks, the carbon-fiber composite socket supplied stiff support and alignment, while the 316L stainless-steel links exhibited adequate structural integrity under varying temperatures.

In addition to the observational studies mentioned before, the prosthetic hand carried out standardized clinical tests, namely the Box and Block Test (BBT) and Jebsen–Taylor Hand Function Test (JTHFT), to allow a

quantitative assessment of its functional performance. The BBT consisted of the user moving blocks across a partitioned box with an overall count of blocks effectively moved registered over the 60-second time period and compared against normative data for transradial prosthetic users. The JTHFT, on the other hand, consisted of seven tasks replicating everyday tasks like turning pages, feeding, and picking up small objects. These assessments highlighted the dexterous performance of the prosthetic hand in carrying out tasks with precision and stability, thereby aiding in the ergonomic and biomechanical assessment of the design. In sum, the combination of real international usage trials and scientific evidence (illustrated by Figure 6) establishes the functional capability, reliability, and user compatibility of the prosthetic hand, thus certifying it as an option for promoting the daily independence of the partial hand amputees.

Kinematics of the Joint under Varying Load Conditions

Analysis of the Angular Displacement Behavior of the Joint Under Varying Load Conditions

The second joint of the prosthetic finger, otherwise known as Joint 2, was subjected to five different levels of external forces while having a two-second actuation time and was prompted to undergo angular displacement curves shown in Figure (6). The levels of external forces applied include 0 N, 10 N, 30 N, 50 N, and 100 N. It should be noted that the linear actuator is powered by a constant speed of 5 mm/s downward while simulating a realistic human-like grasping operation of the fingers with a step term in downward contraction of the finger structure.

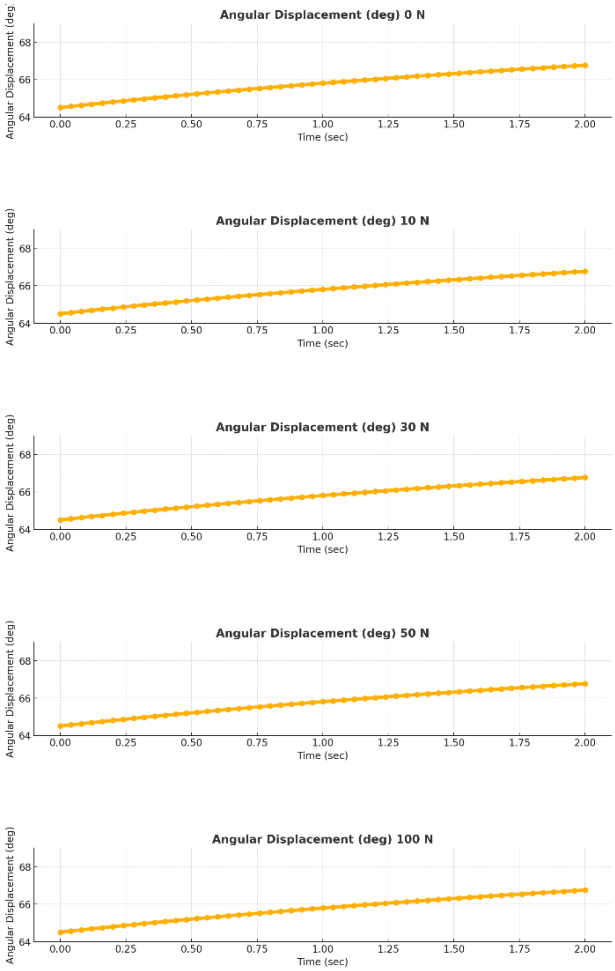

Figure 6. The angular displacement behavior of the joint under varying load conditions

The evaluation showed that angular displacement for this joint remained almost the same under any condition of loading. The deviation of the displacement curves was limited to not greater than about 2 degrees (between about 64.5° and 67.5°), thus proving joint stability even under increasing external load. Such stable functioning owes to a great number of factors entangled with each other. Also, the mechanism operates through kinematic drive mechanisms. The artificial finger uses geometric constraint linkages through which a rigor linear input

drives a mechanical pathway. Finally, the terminal angular position of the joint is dependent on the actuator motion instead of the external force applied to it. This brings the systems into a position-controlled mode, in which displacement is fixed by an input motion and not by an external load response.

The stability of the second joint also corresponds to the material properties of the second joint, which is made of stainless steel 316L. It consists of linkages of stainless steel 316L to create stiffness, good resistance to deformation while being under mechanical loading, and ultimate tensile strength of up to about 485 MPa. With these properties, it reinforces the structural stiffness of the joint during operation while preventing unwanted flexions or shrinkages and hence retaining the desired kinematic path of movement.

Also, the absence of elastic or compliant links such as springs or silicone components in the series of linkages indicates that joint movement is governed solely by the stiffness of the metal frame. This configuration excludes absorption or dissipation of forces by bending elements and requires exact and direct transmission of motion. Lastly, a rigid mechanical link between the metallic arms applying fitting pin joints restrains any variation of motion transfer from base to joint, thus ensuring kinematic stability and output consistency. For the above reason, one can clearly state that the mechanical design of the second joint in stainless steel 316L allowed repeatable and consistent angular motion that shows little sensitivity to loading conditions. This kind of behavior is extremely desirable in prosthetic applications, where precision and consistency of motion are key design requirements.

Analysis of the Angular Velocity Behavior of the Joint Under Varying Load Conditions

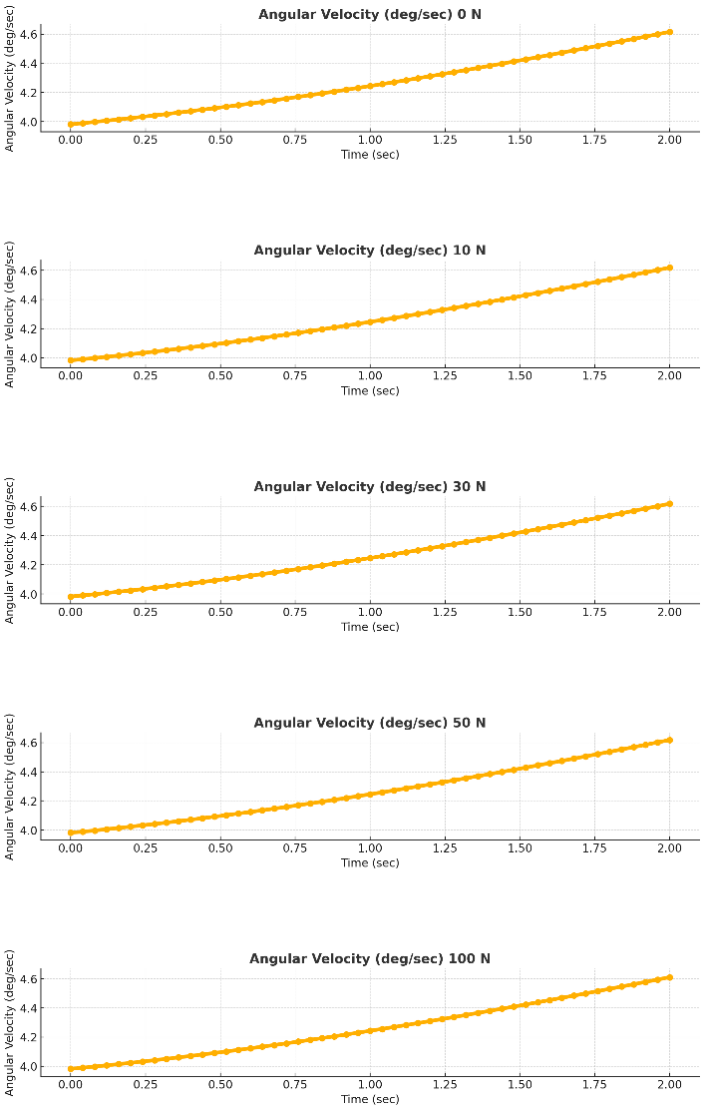

Figure 7. The angular velocity behavior of the joint under varying load conditions

In Figure 7, the angular velocity profiles Joint 2 of a prosthetic finger with respect to two seconds of actuation time. The loading conditions applied in this experiment were: 0 N, 10 N, 30 N, 50 N, and 100 N. The downward movement was implemented with a linear actuator moving downwards at a constant speed of 5mm/s, which would simulate the anatomically realistic grasping motion of a human finger, wherein the tendon-like system is contracted incrementally.

The resulting traces between the angular velocity and the load levels can be described as being exceedingly uniform with hardly distinguished performance. In all the instances, the angular velocity, initially at about 4.0 deg/s, climbs slightly over the 2 seconds to about 4.6 deg/s at the end of the time interval. This minor increase appears consistent for all load conditions, and it implies that mechanical response of the joint is simply dictated by the rate of actuation and not by the external loading conditions.

This uniformity of angular velocity also gives credence to the rule of roles mechanism. The actuator was designed to impose a fixed-price input, from which the operation of the joint is realized: the typical characteristic of speed in angular turns into here something mandated straight by the imposed linear pace and the kinematic geometry, rather than being modulated using resistive forces or dynamic interactions with the load. The use of stainless-steel 316L in the joint and link fabrication also largely contributed toward this behavior. Because of high stiffness characteristics that this material possesses and also a potential loss in structure deformation with applied load, no great lag or damping occurs in the mechanical chain. Therefore, the machine keeps consistent angular velocity switch moving from linear input to joint rotation during increased loads.

Additionally, having no damping components, springs, or elastoplastic materials shows that the whole setup cannot adapt to loads. This reinforces the load-independent angular speed found and confirms that the dynamic reaction of the joint remains stable and predictable during each phase of operation. Ultimately, it can be said that Joint 2 has very stable angular speed profiles at different load conditions due to the rigid, geometrically driven structure of the mechanism combined with the use of stiff-high materials such as stainless-steel 316L. It is this that enhances the reliability of the device being used for prosthetic purposes, ensuring that movement is predictable and can be repeated irrespective of external resistance.

Analysis of the Angular Acceleration Behavior of the Joint Under Varying Load Conditions

In Figure 8, the angular acceleration curves related to the second joint in the prosthetic finger are drawn during the 2nd actuating period stamped by fixed duration of 2 sec, which was tested on 5 different external loading conditions: 0 N, 10 N, 30 N, 50 N, and 100 N. The affector gets activated through a linear actuator operating at a sustained speed of 5 mm/s downwards, which emulates the real natural greedy action of a human finger during flexion movement for instance showing it is flexing.

Angular acceleration seems to have been restricted to a fairly small but steadily increasing range throughout observation, with increases observed from about 0.2 deg/sec² around mid-observation to about 0.35-0.4 deg/sec² toward the end of the test. Trends appear to be fairly similar across all load levels, indicating uniform dynamic response. There seems to be some irregularity in the 0 N curve around mid-time, where some minor fluctuations were observed perhaps because of the lack of any external resistive force that could have helped stabilize the mechanical motion.

Another piece of evidence for a steady angular acceleration pattern adds classification to the machine as a control-function kinematic mechanism, one where the motion output is governed by the imposed linear displacement rather than any externally applied force on the system. Since the angular velocity (which was analyzed earlier) increased uniformly with time, so also the angular acceleration, being the time derivative of velocity, would be expected to have a corresponding linear or quasi-linear trend of increase.

The uniformity of dynamic response comes from the predictable nature of changes in the stress across the mechanism, facilitated by the construction of joints from 316L stainless steel. Due to its high stiffness and resistance to mechanical deformation, disturbances to motion transfer - such as oscillations or lag-any - may be avoided, resulting in smooth and predictable acceleration profiles. The absence of elastic or damping elements in the mechanism further consolidates this behavior, whereby angular acceleration is almost completely controlled by actuator displacement rate and is not affected by variable resistance due to elastic compliance.

On the whole, Joint 2 shows a good and predictable angular acceleration response to applied external loads throughout its range. This pattern is evidence of good machine design and further suggests an overall robustness of this particular prosthetic mechanism for applications demanding smooth, repeatable movement for functionality and confidence within the individual.

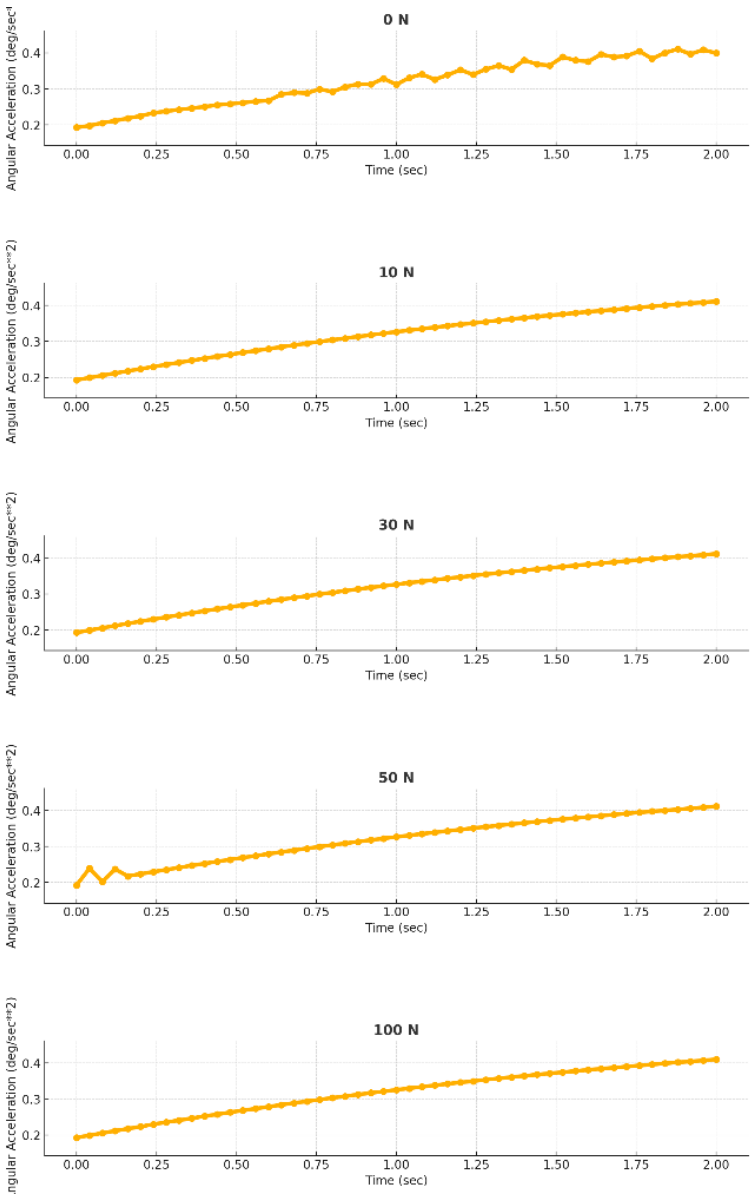

Figure 8. The angular acceleration behavior of the joint under varying load conditions

Analysis of Reaction Force Behavior at the Joint Under Varying Load Conditions

Unloading conditions under which the pressure at Joint 2 of the prosthetic finger was recorded are shown in figure (9): 10, 30, 50, and 100 N. The measurement took place over a time period of 2 seconds while being pushed downwards by a linear actuator at a constant speed of 5 mm/s, a condition chosen to mimic the action of finger flexion during grasping.

The characterization of various arts gives us a clear insight into a systematic way where the acting force upon the joint is maximum at the onset of actuation and uniformly decreases over time for every level of load. For a 10 N load, the response pressure starts low (ca. 0.2 N) and remains almost the same, whereas for a load of 100 N, it kicks off at over 1.5 N and shows decreasing behavior toward the end of the motion. This behavior is indicative of the redistribution of internal forces in the linkage mechanism, as the finger configuration moves from an initial loaded pose toward a more robotic-aligned arrangement in the path of the motion.

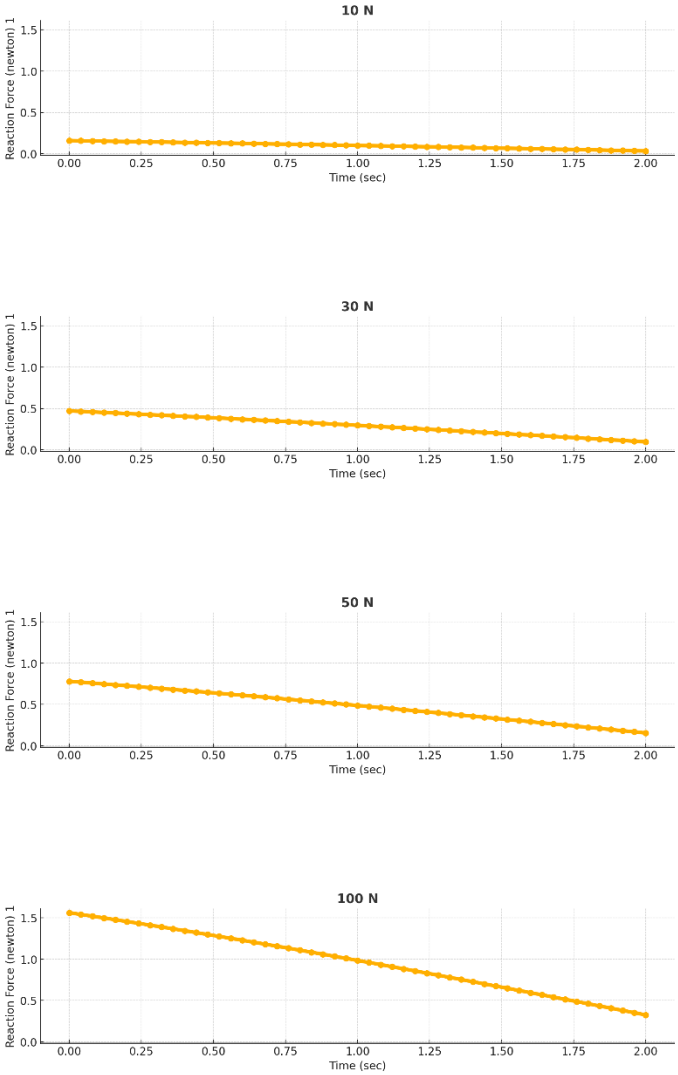

Figure 9. The reaction force behavior at the joint under varying load conditions

Two prominent reasons are given for the decreasing trend of reaction force with time. First, the downward motion of the finger due to the actuator modifies the linkage angular configuration, effectively altering the mechanical advantage and internal moment arms. With these terms, the equality relations of theory could be exploited and verified without being affected by the nonterminal. Second, because the apparatus operates on a position-controlled mechanism, the external load does not affect the path of motion but affects instead the internal force distribution required to maintain that trajectory.

These results also show the load sensitivity of the reaction force as expressed by direct correspondence with applied external pressure and the initial magnitude of the joint reaction. However, due to the rigidity of the system, which is enhanced by the use of 316L stainless steel, and the lack of elastic components, the device maintains a consistent response without oscillations or spikes in force under even high-load conditions.

Overall, the smoothly decreasing Joint 2 reaction force profile under all loading conditions demonstrates the ability of the device to fine-tune internal force transmission according to changing kinematic configurations while preserving mechanical stability. This is a key capability in prosthetic systems, where force modulation is critical to user comfort, device longevity, and safe interaction with objects during real-world use.

Conclusion

The combined motion capability of coupler-based completely absolutely joints allowed stable performance of various types of grips, such as three-finger hold close, pinch grip, and enclosing grip. During these tasks, the

carbon fiber-reinforced composite socket gave reasonable alignment and support management while stainless-steel links in 316L grade encountered just enough structural strain under the different loads.

Beyond observational trials, the prosthetic hand underwent standardized clinical trials using the Box and Block Test (BBT) and the Jebsen–Taylor Hand Function Test (JTHFT) to quantitatively measure functional performance. The BBT test involved a subject passing blocks from one compartment of a box into another with the number of blocks transferred successfully measured within 60 seconds and then compared against normative data for transradial prosthetic users. Similarly, the JTHFT tested seven tasks resembling daily activities, including page turning, simulated feeding, and picking small objects. These tests showed the dexterous capabilities of the prosthetic hand with accuracy and stability, which are design objectives for ergonomic and biomechanical design. In summary, both real-life usage trials and clinical assessments, as described in regard to the prosthetic hand's functionality, reliability, and acceptance by the user, substantiate its contribution to fostering independent living among partial hand amputees.

Recommendations for Future Work

To further develop the prosthetic finger device, several strategic enhancements can be employed in the future. One of them is to integrate low-rate remarks sensors, including stress or electromyographic (EMG) sensors, where customers can receive tactile or muscular reaction in real time. This would make it intuitive and more operative. Another one is automatic actuation by miniaturizing servo mechanisms, which would make it change from being completely passive to semi-active, allowing much better motion control. It would also help to undertake clinical trials on a wider and more diverse population of patients to support further validation of the generalizability and long-term usability of the design. Finally, expanding the mechanical design to facilitate multiple arms or a complete prosthetic hand would significantly enhance functionality and significantly broaden its domain of application among users with more complicated hand amputation cases.

Scientific Ethics Declaration

* The authors declare that the scientific ethical and legal responsibility of this article published in EPSTEM journal belongs to the authors.

Conflict of Interest

* The authors declare that they have no conflicts of interest

Funding

* No funding was received

Acknowledgements or Notes

* This article was presented as an oral presentation at the International Conference on Engineering and Advanced Technology (ICEAT) held in Selangor, Malaysia on July 23-24, 2025.

References

Ahmad, M., Balakrishnan, D., Narayan, A., & Naim, H. (2014). Comprehensive rehabilitation of partially amputated index finger with silicone prosthesis: A case report with 3 years of follow up. *Journal of Indian Prosthodontic Society*, *14*(1), 222–226.

Amaya-Rivas, J. L., Amaya-Rivas, M. A., Amaya-Rivas, D. A., & Amaya-Rivas, J. M. (2024). Future trends of additive manufacturing in medical applications: An overview. *Heliyon*, *10*(5), e26641.

Bashir, T., Ahmad, N., Ahmad, M., Naim, H., & Narayan, A. (2022). Innovative technique for fabrication of

forefinger prosthesis. *Journal of Pharmacy & Bioallied Sciences*, *14*(1), S1033–S1037.

Beckerle, P., Casellato, C., Castaman, A., & Popovic, M. B. (2019). Prosthetic limbs. In M. B. Popovic (Ed.), *Biomechatronics* (pp. 235–278). Academic Press.

Bhaskaran, S., & Zachariah, G. P. (2022). Enhancing retention and esthetics of fabricated silicone finger prosthesis using stump reduction technique and customized acrylic nail: A unique approach. *National Journal of Maxillofacial Surgery*, *13*(1), S140–S144.

Brand, J., Gerez, L., Liarokapis, M., & Pons, J. L. (2019). Improvements on the design of the S-finger prosthetic digit. In L. Masia, S. Micera, M. Akay, & J. L. Pons (Eds.), *Converging Clinical and Engineering Research on Neurorehabilitation III* (pp. 122–126). Springer International Publishing.

Braza, D. W., & Yacub Martin, J. N. (2020). Upper limb amputations. In W. R. Frontera, J. K. Silver, & T. D. Rizzo (Eds.), *Essentials of Physical Medicine and Rehabilitation* (4th ed., pp. 651–657). Elsevier.

Bregoli, C., Gerez, L., & Liarokapis, M. (2022). Osseointegrated metallic implants for finger amputees: A review of the literature. *Orthopaedic Surgery*, *14*(6), 1019–1033.

Cuellar, J. S., Smit, G., Plettenburg, D., & Zadpoor, A. A. (2019). Functional evaluation of a non-assembly 3D-printed hand prosthesis. *Proceedings of the Institution of Mechanical Engineers, Part H: Journal of Engineering in Medicine*, *233*(11), 1122–1131.

Cutipa-Puma, D. R., Coaguila-Quispe, C. G., & Yanyachi, P. R. (2023). A low-cost robotic hand prosthesis with apparent haptic sense controlled by electroencephalographic signals. *HardwareX*, *14*, e00439.

Dunai, L., Novak, M., & García Espert, C. (2020). Human hand anatomy-based prosthetic hand. *Sensors*, *21*(1), 137.

Efanov, J. I., Rizis, D., & Danino, A. M. (2022). A review of utilities and costs of treating upper extremity amputations with vascularized composite allotransplantation versus myoelectric prostheses in Canada. *JPRAS Open*, *32*, 150–160.

Graham, E. M., Lerman, O. Z., & Loeffler, B. J. (2023). From iron hooks to moving hands: The evolution of partial hand prostheses—a surgical perspective. *Orthoplastic Surgery*, *12*, 29–43.

Hall, M. J., Sinskey, Y. L., & Spires, M. C. (2020). Essentials of pediatric prosthetics. *Journal of the Pediatric Orthopaedic Society of North America*, *2*(3), 168.

Hamzah, M., Salman, H. D., & Bakhy, S. H. (2013). An inverse finite element approach for estimating the fiber orientations in intercostal muscles. *2013 IRCOBI Conference Proceedings - International Research Council on the Biomechanics of Injury*, 722–733.

Kamel, S. H., Hamzah, M. N., & Atiyah, Q. A. (2024). Solar trees: Harnessing renewable energy for portable charging of low-capacity devices. *CEUR Workshop Proceedings*, 9–18.

Kamel, S. H., Hamzah, M. N., Abdulateef, S. A., & Atiyah, Q. A. (2023). A novel design of smart knee joint prosthesis for above-knee amputees. *FME Transactions*, *51*(2), 131–139.

Kamel, S. H., Hamzah, M. N., Atiyah, Q. A., & Abdulateef, S. A. (2025). A novel real-time program for predicting the eight walking stages of amputated and healthy person. *AIP Conference Proceedings*, *3350*(1), 70019.

Kerver, N., Twickler, T. B., van der Sluis, C. K., & Postema, K. (2023). Economic evaluation of upper limb prostheses in the Netherlands including the cost-effectiveness of multi-grip versus standard myoelectric hand prostheses. *Disability and Rehabilitation*, *45*(25), 4311–4321.

Kristjansdottir, F., Dahlin, L. B., Rosberg, H. E., & Carlsson, I. K. (2020). Social participation in persons with upper limb amputation receiving an esthetic prosthesis. *Journal of Hand Therapy*, *33*(4), 520–527.

Kumar, A., Patel, S., & Singh, R. (2023). Finger prosthesis: An economic and esthetic approach. *Cureus*, *15*(7), e41989.

Kyberd, P. (2022a). Research in Sweden: The pioneers of paediatric prosthetics and osseointegration. In P. Kyberd (Ed.), *Making Hands* (pp. 253–273). Academic Press.

Kyberd, P. (2022b). Artificial arms. In P. Kyberd (Ed.), *Making Hands* (pp. 7–38). Academic Press.

Munaretto, N., & Loeffler, B. J. (2023). Partial hand amputation: Digital and transmetacarpal amputation. *Operative Techniques in Orthopaedics*, *33*(3), 101059.

Nelson, F., & Blauvelt, C. (2022). Prosthetics and orthotics. In F. Nelson & C. Blauvelt (Eds.), *A Manual of Orthopaedic Terminology* (9th ed., pp. 197–215). Elsevier.

Ornaghi, H. L., Jr., Monticeli, F. M., & Agnol, L. D. (2023). A review on polymers for biomedical applications on hard and soft tissues and prosthetic limbs. *Polymers*, *15*(19), 4034.

Rand, S., Surapaneni, T., Bartels, M. N. M., & Gitkind, A. (2024). Approaches to prosthetic limb restoration in resource-limited settings/countries: 3 dimensional printing. *Physical Medicine and Rehabilitation Clinics of North America*, *35*(4), 897-904.

Salman, H. D., Bakhy, S. H., & Hamzah, M. N. (2020). Contact mechanics for soft hemi elliptical robotic fingertip. *Journal of Mechanical Engineering Research and Developments*, *43*(6), 286–298.

Segil, J. L., Huddle, S. A., & Weir, R. F. (2021). The Point Digit II: Mechanical design and testing of a ratcheting prosthetic finger. *Military Medicine*, *186*(Suppl 1), 674–680.

Semprini, M., Laffranchi, M., De Michieli, L., & Gruppioni, E. (2022). Clinical evaluation of Hannes: Measuring the usability of a novel polyarticulated prosthetic hand. In Q. Li et al. (Eds.), *Tactile Sensing, Skill Learning, and Robotic Dexterous Manipulation* (pp. 205–225). Academic Press.

Sheehan, T. P. (2021). Rehabilitation and prosthetic restoration in upper limb amputation. In D. X. Cifu (Ed.), *Braddom's Physical Medicine and Rehabilitation* (6th ed., pp. 153–173). Elsevier.

Shokur, S., & Micera, S. (2024). Thermal phantom sensations in arm amputees and what it means for future prosthetics. *Temperature*, *11*(2), 107–109.

Sinke, M., Chadwell, A., & Smit, G. (2022). State of the art of prosthesis simulators for the upper limb: A narrative review. *Annals of Physical and Rehabilitation Medicine*, *65*(6), 101635.

Sinskey, Y. L., & Spires, M. C. (2024). Prostheses and rehabilitation principles in pediatric limb deficiency. *Physical Medicine and Rehabilitation Clinics of North America*, *35*(4), 707-724.

Spaulding, S., & Chen, T. (2020). Prosthetic options for persons with upper extremity amputation. In K. K. Chui, M. Jorge, S. Yen, & M. M. Lusardi (Eds.), *Orthotics and Prosthetics in Rehabilitation* (4th ed., pp. 759–783). Elsevier.

Tchurukdichian, A., Gindraux, F., & Loisel, F. (2023). Time to return to work after total trapeziometacarpal prosthesis. *Hand Surgery and Rehabilitation*, *42*(4), 347–353.

Vaskov, A. K., Vu, P. P., & Stephen, N. J. (2022). Surgically implanted electrodes enable real-time finger and grasp pattern recognition for prosthetic hands. *IEEE Transactions on Robotics*, *38*(5), 2841–2857.

Yaseen, M. A. S., Hamzah, M. N., & Kamel, S. H. (2025). Innovations and advances in finger prostheses: A comprehensive review of design configurations in prosthetics. *The International Middle Eastern Simulation and Modelling Conference (MESM 2024)*, 113–118.

Zheng, J. Y., Kaliki, V., & Thakor, N. V. (2019). Priorities for the design and control of upper limb prostheses: A focus group study. *Disability and Health Journal*, *12*(4), 706–711.

Author(s) Information

Mennat Allah S. Yaseen
University of Technology- Iraq, College of Mechanical Engineering, Baghdad, Iraq

Mohsin N. Hamzah
University of Technology- Iraq, College of Mechanical Engineering, Baghdad, Iraq

Shaimaa H. Kamel
University of Technology- Iraq, College of Mechanical Engineering, Baghdad, Iraq
Contact e-mail: *shaimaa.h.kamel@uotechnology.edu.iq*

To cite this article:

Yaseen, M. A. S., Hamzah, M. N., & Kamel, S.H. (2025). Prosthetic finger design for partial hand amputees: A five-bar linkage approach. *The Eurasia Proceedings of Science, Technology, Engineering and Mathematics (EPSTEM), 37,* 962-980.